Phase behavior of blends of PCBM with amorphous polymers with different aromaticity

Gabriel Bernardo,[a] Nabankur Deb,[b] Stephen M. King,[c] David G. Bucknall[b,d,e*]

[a]Institute for Polymers and Composites/I3N, University of Minho - Campus de Azurém, 4800-058 Guimarães, Portugal

[b]School of Materials Science and Engineering; Georgia Institute of Technology, Atlanta, GA 30332, USA

[c]ISIS Neutron Source, STFC, Rutherford Appleton Lab., Harwell, Oxon, OX11 0QX, UK

[d]Center for Organic Photonics and Electronics (COPE), Georgia Institute of Technology, Atlanta GA 30332, USA

[e]Currently at: Engineering and Physical Sciences, Heriot-Watt University, Edinburgh, EH14 4AS, UK

*Correspondence to: David G. Bucknall (E-mail: *bucknall@gatech.edu*)

ABSTRACT:

The phase behavior of [6,6]-phenyl C_{61}-butyric acid methyl ester (PCBM) blends with amorphous polymers with different degrees of aromaticity has been investigated by differential scanning calorimetry (DSC) and small angle neutron scattering (SANS). The polymers investigated are the homologous series of polystyrene (PS), poly(2-vinyl-naphthalene) (P2VN) and poly(9-vinyl-phenanthrene) (P9VPh). The DSC results show that the miscibility of PCBM in these polymers increases non-linearly from 16.5 wt.% in PS, 57.0 wt.% in P2VN and 74.9 wt.% in P9VPh. The SANS results show that at all concentrations of PCBM, the blends are composed of two mixed phases. Analysis shows that the phase dimensions remain largely independent of PCBM content, but there is a strong dependence of the PCBM concentration difference in the two phases with increasing PCBM content.

KEYWORDS: vinyl polymer; PCBM fullerene; miscibility; DSC; SANS

INTRODUCTION

Since their discovery fullerenes have been widely studied and are finding increasing application in numerous technological areas, including in current state-of-the-art polymer photovoltaic devices (OPVs). Following its discovery, pristine fullerene C_{60} was quickly implemented as an electron acceptor in polymer photovoltaic research.[1, 2] However, C_{60} is insoluble or only poorly soluble in most common organic solvents, and only poorly miscible in conjugated polymer matrices, limiting its ability to be incorporated in commercial products. An important

breakthrough in polymer photovoltaic devices was achieved when pristine fullerene C_{60} was replaced by its highly soluble derivative PCBM ([6,6]-phenyl C_{61}-butyric acid methyl ester).[3]

At present there is a race to develop novel conjugated polymers (electron donors) that can further improve the efficiency of polymer solar cells. Despite this, PCBM remains the most popular electron acceptor material for organic solar cells, although there are question marks over just how chemically compatible PCBM is with the huge diversity of donor polymers. The frequently observed poor device performance, when testing new polymers with PCBM, might be partially related to a chemical incompatibility

between the polymer and PCBM. Furthermore, it has been recently recognized that the solubility of a fullerene derivative strongly affects the morphology of its composite with poly(3-hexylthiophene) (P3HT), which is commonly used as active material in bulk heterojunction organic solar cells. Troshin et al.,[4] have shown that there is a general dependence of all solar cell parameters (short circuit current, J_{SC}, open circuit voltage, V_{OC}, fill factor, *FF,* and power conversion efficiency, η) on the solubility of the fullerene derivative used as an acceptor component in the photoactive layer of an organic solar cell. According to these authors, the best material combinations are those where donor and acceptor components are of similar and sufficiently high solubility in the solvent used for the deposition of the active layer. In order to improve the chemical affinity between the fullerene and the polymer, and ultimately improve the underlying morphology as well as the device efficiency, one strategy has been to functionalize the C_{60} donor.[5-10] A different strategy has been to alter the pendant groups in the polythiophene acceptor.[11] For all these reasons, there is therefore a current need for a greater fundamental understanding of the interactions between the fullerene derivatives and the polymers.

Compelled by the increasing evidence relating fullerene solubility with solar cell performance, several authors have studied the miscibility and phase diagrams of several PCBM blends.[11-17] These have included PCBM blends with polythiophenes (P3BT, P3HT, P3DDT),[11-14] with polyphenylene vinylenes (PPVs)[12, 15] and with poly(3-hexylselenothiophene) (P3HS).[16] Kim et al.,[12] using a combination of X-ray diffraction (XRD) and differential scanning calorimetry (DSC), studied the phase behavior of PCBM with P3HT, MDMO-PPV and MEH-PPV and determined the solubility limits of PCBM in these polymers to be 30, 40 and 50 wt% respectively. Müller et al.,[11] using a combination of DSC, optical microscopy and XRD, studied the phase behavior of PCBM with P3BT, P3HT

and P3DDT. Zhao et al.,[13] measured the phase diagram of P3HT:PCBM blends using conventional and modulated temperature DSC (DSC and MTDSC) and investigated PCBM blends with PPV polymers[15] using these same techniques and rapid heat-cool calorimetry (RHC). Hopkinson et al.,[14] measured the phase diagram of P3HT:PCBM blends using dynamic mechanical thermal analysis (DMTA). Ballantyne et al.,[16] studied the phase diagram of PCBM with poly(3-hexyl-selenothiophene) (P3HS) using a combination of DSC, XRD, optical microscopy and Raman imaging. Quantitative structure-property relationships (QSPRs) between the molecular structure of fullerene derivatives and their solubility in chlorobenzene have also been recently established.[18]

Previous studies on the phase behavior of PCBM:polymer blends using DSC have relied mainly on the tracking of variations of the glass transition temperature (T_g) and on the identification of either one single T_g (one-phase system) or of two different T_gs (two-phase separated system). However previous studies in PCBM:P3HT blends have shown that experimentally measured glass transition temperatures are subjected to large experimental uncertainties.[13] Furthermore, the measurement of T_g is highly dependent on the measurement technique. According with Zhao et al.,[13] the T_g of the PCBM:P3HT system, as determined using DSC and MTDSC, increases from 12.1 ℃ for pure P3HT to 131.2 ℃ for pure PCBM. According to Hopkinson et al.,[14] using dynamic mechanical thermal analysis (DMTA), the T_g increases from ~40℃ for pure P3HT to ~70℃ for a PCBM load of 65 wt.% and then drops between 70 and 75 wt.% indicating phase separation.

Following our previous preliminary study,[19] this work focuses on the study of the phase behavior of PCBM blends with amorphous polymers of different aromaticity, namely polystyrene (1 aromatic ring), poly(2-vinyl-
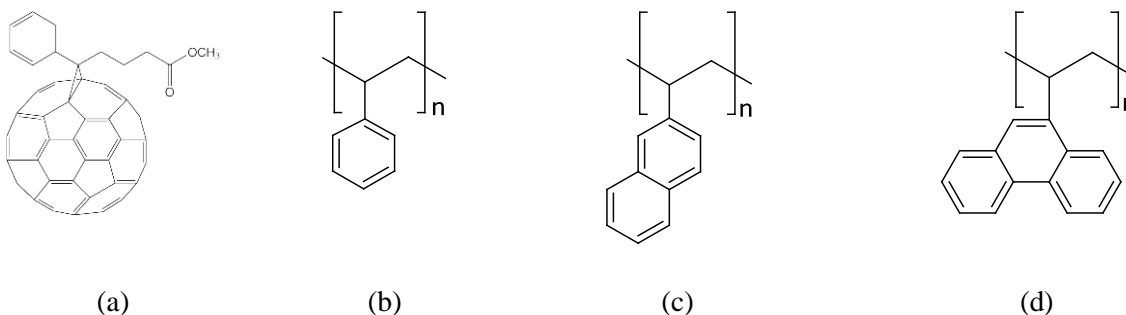
Figure 1. Chemical structures of PCBM and of polymers investigated experimentally with PCBM for effects of increased aromaticity on dispersion: (a) PCBM, (b) PS, (c) P2VN and (d) P9VPh.

naphthalene) (2 fused aromatic rings) and poly(9-vinyl-phenanthrene) (3 fused aromatic rings). It is our ultimate goal to understand how aromaticity affects the phase behavior of the PCBM-polymer blends. By comparison with a previous study on pristine C_{60} in PS, P2VN and P9VPh,[20] we also aim to understand the effect of the PCBM pendant group on the PCBM miscibility and dispersibility.[21]

EXPERIMENTAL

Materials and Sample Preparation
[6,6]-phenyl C61-butyric acid methyl ester (PCBM) was purchased from American Dye Source (A.D.S.). Atactic polystyrene (PS) (M_w = 115k g/mol; M_n = 109k g/mol), poly(2-vinyl-naphthalene) (P2VN) (M_w = 72k g/mol; M_n = 45 k g/mol) and poly(9-vinyl-phenanthrene) (P9VPh) (M_w = 7.7 k g/mol; M_n = 6.8 k g/mol) were all purchased from Polymer Source Inc.. Whilst these polymers have different molecular weights, we have seen in previous studies with C_{60}, that molecular weight differences only make a small variation to the miscibility limit.[20] Blends of the polymers with PCBM were all made by initially dissolving each polymer and the PCBM separately in toluene at concentrations of about 1 wt. %, i.e. well below the solubility limit for each material, and sonicating until dissolved, i.e. typically for a minimum of 20 minutes. Subsequently, the two solutions were mixed to obtain the required ratios of polymer:fullerene. After sonication of the mixed solution for another 20-30 minutes, the blend was precipitated in to an excess of rapidly stirred cold methanol, vacuum filtered using a nylon membrane filter with pore size

0.45 μm (Whatman, cat nº 7404-004) and washed with cold methanol. The solids were then dried in a vacuum at ~70 ºC for several hours until no mass changes were detected and then stored for subsequent measurements. The chemical structures of PCBM and the conjugated polymers are shown in Figure 1.

DSC Measurements
DSC measurements of the blends and pure compounds were made in standard mode on a TA Instruments Q200. Argon with a flux of about 50 mL min^{-1} was used as a purge gas. About 5 mg of each sample was sealed in aluminum crucibles (Perkin Elmer kit nº 0219-0041). The scan rate was 10 Kmin^{-1}. Two heating-cooling cycles were run between the temperatures of 20ºC and 300ºC. The stay time at each of these extreme temperatures was 3 minutes. The first heating curve was slightly different from the subsequent heating curve due to the complex thermal history of the as-prepared samples and their poor contact with the crucibles in the first heating. Only the data determined from the first cooling and the second heating cycles were used in the subsequent discussion, since these data represent the samples that are at thermodynamic equilibrium.

SANS Measurements
Small angle neutron scattering (SANS) data from solid films of the blends were acquired on the diffractometer LOQ at the ISIS Facility (Didcot, UK).[22] Due to the high carbon to hydrogen content in PCBM, they have a naturally high neutron scattering density contrast with the hydrogenous polymers, so that no isotopic substitution was required. Data were

obtained from samples containing weight fractions of PCBM above and below the critical miscibility limits of the three polymers as determined by DSC analysis. The powders from each sample were pressed into discs in an IR disc press at room temperature using a 2 ton load. The samples were prepared to be approximately 1 mm thick, although their exact thickness was measured by micrometer and that value used in the data reduction procedure to ensure proper scaling. The samples were annealed in situ in the LOQ instrument for several hours before data were collected at 225 °C. Although, not an exact thermal match compared to the DSC, given other data, the time scale of annealing and the temperature at which we measured it is believed that these data are close to the thermodynamic equilibrium for this system.

LOQ is a fixed-geometry "white beam" time-of-flight instrument which at 25 Hz utilizes neutrons with wavelengths, λ, between 2 and 10 Å. Data are simultaneously recorded on two, two-dimensional, position-sensitive, neutron detectors, to provide a simultaneous q (the scattering vector, $= 4\pi/\lambda \sin \theta/2$, where θ is the scattering angle) range of $0.008-1.6$ Å^{-1}. Each blend sample and background sample was measured for typically 1 or 2 hours in order to gather data of high statistical precision. Each raw scattering data set was then radially-averaged, corrected for the detector efficiencies, sample transmission and background scattering and converted to scattering cross-section data, i.e. absolute scattering intensity, $(\partial\Sigma/\partial\Omega$ vs $q)$ using the instrument-specific software.[23] The absolute scattering was calibrated using the scattering from a standard sample (a solid blend of hydrogenous and perdeuterated polystyrene) in accordance with established procedures.[24] The data were then fitted to appropriate models using SasView (Version 3.1.1).[25]

RESULTS AND DISCUSSION

Fig. 2 shows DSC thermograms of blends of PCBM with three different vinyl polymers: PS, P2VN and P9VPh, over a wide composition range. All three pure polymers are amorphous, thus neither melting nor crystallization can be

seen on their corresponding thermograms. Pure PCBM is semicrystalline and shows two melting peaks with the main peak at higher temperature and the smaller peak at lower temperature, in agreement with literature.[11, 13, 26] Therefore, for all the PCBM:polymer blends with different compositions, both the crystallization and melting peaks can be attributed to PCBM.
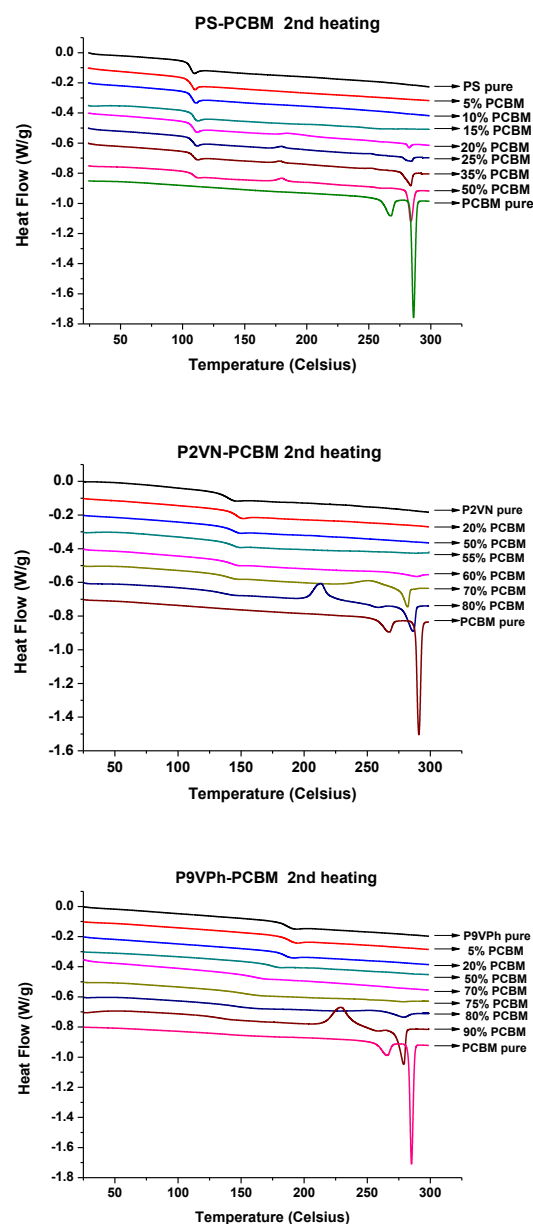

Figure 2. DSC thermograms of PS-PCBM, P2VN-PCBM and P9VPh-PCBM blends, as a function of PCBM concentration. DSC traces have been translated vertically for clarity.

Table 1. Area under PCBM melting peaks, A_{melt} (J/g), determined from DSC measurements as a function of weight percentage of PCBM, x (wt. %).

PS + x.PCBM		P2VN + x.PCBM		P9VPh + x.PCBM	
x (wt.%)	A_{melt} (J/g)	x (wt.%)	A_{melt} (J/g)	x (wt.%)	A_{melt} (J/g)
20	0.603	60	1.212	75	0.352
25	1.385	80	6.713	80	2.464
35	3.190	100	13.850	90	7.735
50	5.404	-	-	100	13.850
100	13.850	-	-	-	-

For all these systems the polymer glass transition temperatures are clearly visible (Figure 2). For the PS blends, the PS glass transition temperature increases only very slightly with the increase in PCBM load. For the P2VN blends, the T_g increases a few degrees, up to 20 wt.% PCBM load but then decreases at higher PCBM loads returning to T_g values very similar to the values of the pure polymer. For the P9VPh blends the T_g remains approximately constant up to 20 wt.% loading, but then decreases considerably at higher PCBM loads.

These observations, for all the systems, contrast with previous observations in blends of PCBM with conjugated polymers (namely P3HT) in which much larger variations in T_g (from 12.1°C for pure P3HT to 131.2°C for pure PCBM) have been observed.[13]

With the addition of polymer, the crystallinity of PCBM decreases significantly. As shown in Fig. 2 a cold crystallization peak appears in the second heating for all the blends above a critical weight fraction of PCBM. It is assumed that the appearance of this cold crystallization peak together with the PCBM melt peak is indicative of the formation of pure phases of PCBM. For the PS blends, the cold crystallization peak appears at approximately 180 °C and together with the observation of a PCBM melt peak occurs at a critical value of PCBM between 15 and 20 wt.%. For the P2VN blends, the first observable melt peak is just observable for 60

wt.% PCBM blends. This indicates that the critical miscibility is just below 60 wt.% PCBM. For the P9VPh blends, a broad melt peak is observed for the 80 wt.% PCBM sample, with a much weaker peak just observable at 75 wt.% loading. This indicates the miscibility limit is just below this composition.
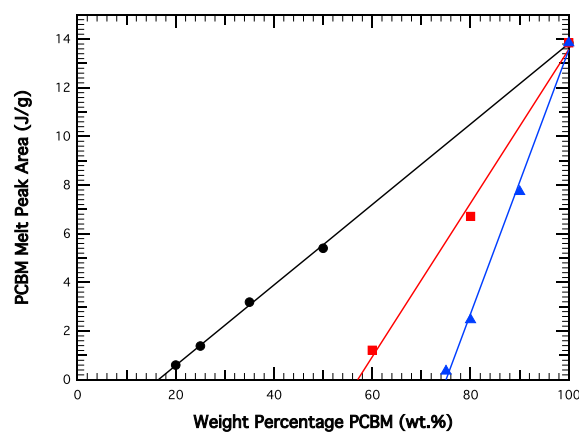

Figure 3. Area under the PCBM DSC determined melting peaks for PS (●), P2VN (■) and P9VPh (▲) blends as a function of PCBM content. Solid lines are linear fits to the data.

A better measure of the limit of miscibility of PCBM in each of the polymers, was established by determining the areas under the PCBM melt peak and plotting as a function of PCBM. Therefore we are defining the limit of miscibility as the point at which no pure PCBM phases are observed in the system, within the limits of

resolution by the DSC. The extracted values of peak areas are given in Table 1, and plotted in Figure 3.

Using the value for pure PCBM and extrapolating the values of peak area for each of these polymer blends to a zero peak area, the values of the miscibility limit of PCBM in the three polymers can be determined. Using this approach, we obtain PCBM miscibility limits of 16.5 wt.% in PS, 57.0 wt.% in P2VN and 74.9 wt.% in P9VPh. These values are considerably higher than previous results obtained for solubility of C_{60} in the same polymers,[20] as shown in Figure 4. The interaction between the vinyl polymers and C_{60} was seen to be largely associated with the phenyl side groups. Clearly the presence of the ligand in PCBM onto the fullerene cage introduces a strong interaction with the phenyl groups, rather than the polymer backbone. These results also support recent observations,[27] which showed that despite PCBM possessing lower thermal and thermo-oxidative stability than C_{60}, composites of polystyrene with PCBM have higher thermal and thermo-oxidative stabilities than the corresponding composites with C_{60}. This apparent contradiction has been attributed to a higher miscibility limit of PCBM in polystyrene compared to that of C_{60}.
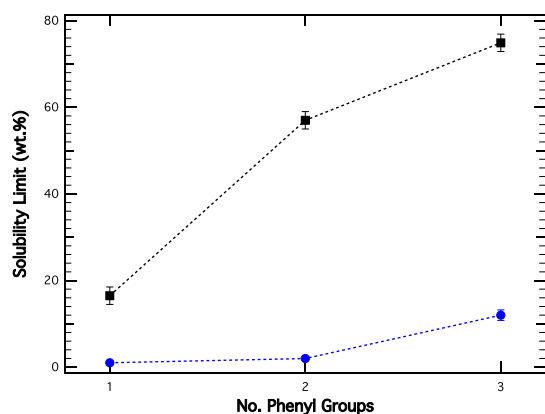

Figure 4: Solubility limit of PCBM (■) compared to C_{60} (●) for PS, P2VN and P9VPh. Data for C_{60} miscibility are from taken from reference [20].

We have also used SANS measurements to investigate the effect on phase behavior with increasing PCBM content.[28] Although not reported here, evidence from SANS data taken at higher annealing temperatures than the data reported in this paper, indicates that these samples are close to thermodynamic equilibrium. Consequently, the SANS and DSC results are comparable, but since the samples used in each technique have undergone a different thermal history it must be remembered that the results cannot be exactly correlated.

The magnitude of the scattering cross-section (intensity) in SANS is proportional to the number, size and 'visibility' (contrast) of the scattering entities in a sample, whilst the q-dependence of the cross-section is related to their shape and local arrangement. A representative set of SANS data, in this case for the polystyrene-PCBM blends are shown in Figure 5. For these, and also the P2VN and P9VPh blends, the scattering shows similar behavior, displaying an increase in intensity with decreasing q. This indicates that neutrons are being scattered from relatively large characteristic length scales (of the order $2\pi/q$).
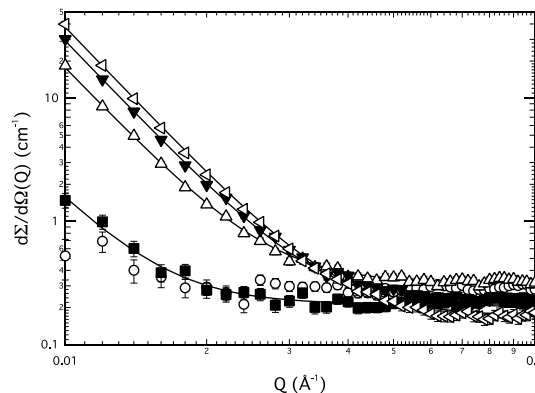

Figure 5: Radially averaged 1D absolute small angle scattering intensity as a function of scattering vector for PS-PCBM blends at 0 (○), 10 (■), 15 (△), 20 (▼) and 25 (◁) % PCBM content. The solid lines represent fits to the data using the DB model (Equation 1).

The scattering in the pure polymers show a different behavior compared to the blends. The scattering is very weak even at the lowest q values, and is likely to result from density fluctuations in the sample. The scattering is

therefore weaker than the blends because the neutron scattering contrast is smaller in the pure polymers. The different q-dependence in the blends indicates that the scattering primarily arises from the PCBM as well as any change in the local arrangement of the PS the PCBM imposes. This is further confirmed by the observation that the intensity at low-q increases with increasing PCBM volume fraction, ϕ_{PCBM}. At values of ϕ_{PCBM} above the DSC determined miscibility limit the scattering intensity does not increase significantly at low-q.

A simple power law fit to the low-q data shows that in all but the pure polymer samples the intensity decays with a power law relationship proportional to $q^{-\alpha}$, with α between 2.8 and 3.8. This suggests that the underlying morphology of the samples is fractal and composed of distinct regions delineated by boundaries with some roughness. With this in mind we initially fitted the data to a scattering law variously called the Debye-Bueche (DB) or Debye-Anderson-Brumberger (DAB) model. This has the form:[29, 30]

$$\frac{d\Sigma}{d\Omega}(q) = \frac{c_{DB}L^3}{(1+(qL)^2)^2} + b \qquad [1]$$

where the scaling factor $c_{DB} = 8\pi(\Delta\rho)^2\phi_1\phi_2$, and $\Delta\rho$ is the neutron scattering length density difference between two randomly distributed phases with volume fractions of ϕ_1 and ϕ_2 that are characterized by a single average density correlation length, L, which is essentially the average separation between the phases. The second term on the right hand side of the equation, b, is the background intensity that includes both instrumental and sample specific factors, i.e. the incoherent scattering intensity. From Figure 5, it is seen that the DB model is a reasonably good description of the data at all concentrations for all three polymers. The values obtained from the fitting for $\Delta\rho$ and L using Equation 1 are given in Table 2.

It can be seen that with increasing PCBM the value of $\Delta\rho$ between the two phases increases. For compositions below the DSC determined miscibility values, the values of $\Delta\rho$ are very small indicating that the 'two phases' have very

similar compositions. The two regions we are observing are therefore more like compositional density fluctuations than true phase domain structures. It is not clear what the origin of these fluctuations is at present, and the focus of additional studies. For each of the polymers, the values of $\Delta\rho$ are seen to increase significantly around the values of the miscibility limits determined by DSC (see Figure 6). Interestingly, the magnitude of $\Delta\rho$ at ϕ_{PCBM} above the miscibility limit are relatively small, reaching a maximum in the P2VN blends of $\Delta\rho = 2.81\times10^{-6}$ Å^{-2}. Above the miscibility limit in each blend, the PCBM forms pure crystals, which has a scattering length density, $\rho = 4.34 \times10^{-6}$ Å^{-2}, and that of the vinyl polymers is range from 1.4×10^{-6} to 1.9×10^{-6} Å^{-2}. Consequently, the low values of $\Delta\rho$ in the blends even in the phase separated compositions, indicates that the polymer blend is composed of pure PCBM crystal aggregates in a matrix itself composed of amorphous polymer with dispersed fullerene.

A weakness with using DB analysis is that it is a shape-independent model and in that respect provides rather limited system specific information. However, we know more about the system than the fact that it is simply two-phase, particularly since we suspect the presence of PCBM 'clusters' in the blends as have been advocated by other researchers. A more sophisticated model would combine the scattering from a fractal morphology with that from particulate clusters, and this is the basis of what is called the Mass-Fractal (MF) model. This defines the scattering in terms of fractal aggregates consisting of spherical primary particles of radius R, such that:[31]

$$\frac{d\Sigma}{d\Omega}(q) = c_{MF} \frac{3[\sin(qR)^2 - (qR)^2\cos(qR)^2]}{(qR)^6}$$

$$\times \frac{\Gamma(D_m-1)\zeta^{(D_m-1)}}{[1+(q\zeta)^2]^{\frac{(D_m-1)}{2}}} \cdot \frac{\sin[(D_m-1)\tan^{-1}(q\zeta)]}{q} + b$$

$$[2]$$

where D_m is the mass fractal dimension, ζ is the fractal cut-off length, and c_{MF} is a scale factor

that is also proportional to $(\Delta\rho)^2$. The MF model is, however, extremely sensitive to these three parameters if they are fitted as independent variables. Given we suspected the presence of PCBM aggregates we have fitted the data using Equation 2 assuming a fixed value of $R = 5$ Å, *i.e.* the approximate equivalent spherical radius for a PCBM molecule. Using this assumption the MF model also gives equally good fits to the SANS data. The derived parameters are shown in Table 3.

Clearly by fitting the data using both the DB and MF models suggests that for all three polymers at all compositions both above and below the miscibility limit (determined from the DSC measurements) the blends are composed of two phases, but of varying composition. This behavior indicates that the systems are not at equilibrium, as may be anticipated from the sample preparation method for the SANS samples. The question remains about what the apparent phases are composed of and consequently what are the origins of the observed concentration dependent changes seen in the scattering data. A route to understand this is behavior is to explore the behavior of the fitting parameters more deeply.

From fits to the DB model it is seen that for all three polymers the value of L is reasonably large

(of order of hundreds of Ångstrom). This observation is mirrored by the results from the MF model. The values of ζ are broadly comparable to the L values and generally reflect the same changes with PCBM content, although there are no systematic changes seen in the values of L or ζ with increasing ϕ_{PCBM} from either model fit. However, as shown in Figure 6, the variation in DAB scaling factor (c_{DB}) for all the polymer systems shows clear non-linear increases with PCBM concentration.

Although not shown, similar increases in the scale factor (c_{MF}) are also observed from fits to the mass-fractal model (Equation 2). The largest values of c_{DB} are seen in the PS system and are smallest for the P9VPh system. Since c_{DB} is proportional to the scattering length density difference between phases it is clear that at these maximum values greater mixing in the systems is observed in the P9VPh compared to P2VN, which in turn is more miscible than the PS system. This ties in with the L values, which are smaller in the P9VPh system at 70-80% PCBM loading than they are in the P2VN system. For the PS-PCBM system there is a distinct upturn in the c_{DB} at a PCBM concentration that is consistent with the miscibility limit determined by the DSC crystalline-peak area disappearance. At these concentrations pure PCBM crystals are

Table 2: Scattering length density differences and correlation lengths for vinyl polymer-PCBM blends determined using DB model (Equation 1) fits to the SANS data taken at 225 °C.

PS+PCBM			P2VN+PCBM			P9VPh+PCBM		
ϕ_{PCBM}	$\Delta\rho$ (Å^{-2})	L (Å)	ϕ_{PCBM}	$\Delta\rho$ (Å^{-2})	L (Å)	ϕ_{PCBM}	$\Delta\rho$ (Å^{-2})	L (Å)
0.10	1.92×10^{-7}	582 ± 427	0.20	6.73×10^{-8}	66.7 ± 19.5	0.05	1.85×10^{-7}	71.6 ± 2.7
0.15	8.47×10^{-7}	1312.0 ± 17.6	0.55	2.03×10^{-6}	1391.5 ± 4.1	0.20	4.26×10^{-8}	369.8 ± 108.8
0.20	9.72×10^{-6}	1295.5 ± 11.8	0.60	2.12×10^{-6}	1360.7 ± 3.9	0.70	7.49×10^{-7}	427.4 ± 13.0
0.25	1.02×10^{-6}	1306.0 ± 10.0	0.70	2.81×10^{-6}	1400.3 ± 3.3	0.80	1.26×10^{-6}	486.4 ± 1.0

observed in the system (as determined by DSC), so the upturn in c_{DB} is associated with formation of PCBM crystals and PS-rich (PCBM depleted) domains forming above this critical concentration. Although c_{DB} increases for the P2VN and P9VPh system with increasing PCBM concentration there is no apparent faster

increase observed above the critical values determined by DSC. This is presumably because of the difference in miscibility of PCBM in these two polymers compared to PS, so that even though PCBM-phases are formed, the degree of PCBM in the remaining matrix of the system remains high.

Table 3: Mass fractal dimensions, and fractal cut-off lengths determined using MF model fits (Equation 2) to the SANS data taken at 225 °C, assuming a primary particle radius of 5 Å.

PS+PCBM			P2VN+PCBM			P9VPh+PCBM		
ϕ_{PCBM}	D_m	ζ (Å)	ϕ_{PCBM}	D_m	ζ (Å)	ϕ_{PCBM}	D_m	ζ (Å)
0.10	3.02 ± 0.04	399.9 ± 42.7	0.20	2.82 ± 0.27	74.7 ± 16.9	0.05	3.07 ± 0.01	59.0 ± 3.1
0.15	3.03 ± 0.01	386.6 ± 6.1	0.55	3.02 ± 0.02	410.8 ± 1.3	0.20	3.03 ± 0.09	313.8 ± 67.5
0.20	3.00 ± 0.01	378.8 ± 4.0	0.60	3.02 ± 0.02	415.7 ± 1.3	0.70	2.99 ± 0.01	362.8 ± 0.9
0.30	3.03 ± 0.01	395.3 ± 3.5	0.70	3.01 ± 0.01	397.9 ± 1.0	0.80	3.07 ± 0.01	325.9 ± 0.6

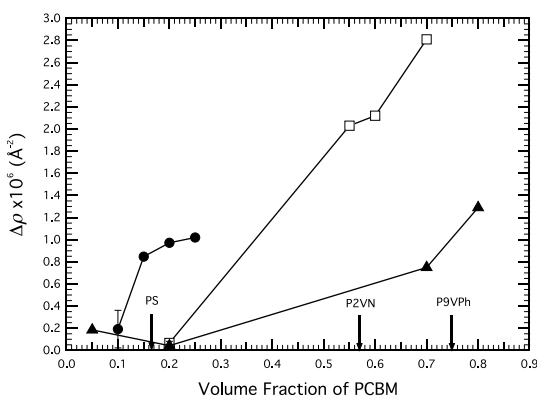**Figure 6:** Plot of DAB-model scale factor (derived using fits to from Equation 1), as a function of PCBM concentration for PS ($\bullet$), P2VN ($\square$) and P9VPh ($\blacktriangle$). The arrows indicate the miscibility limit determined by DSC from crystalline-peak area analysis.

As shown by the fractal dimension values for all, MF fits are approximately 3 for all three

polymers at all concentrations. The scattering behavior from fractals follows a q^{-D_m} scattering dependence for $q < \zeta^{-1}$, and changes to q^{D_m-6} for $q > \zeta^{-1}$.[31] Given the values of ζ (Table 3) we can expect from the fitting results where $D_m \sim 3$ to observe a q^{-3} scattering dependence. This is consistent with the observed scattering power law dependence observed where we obtained a $q^{-2.8}$ to $q^{-3.8}$ behavior. This indicates that at the length scales we are observing the interfaces between the phases are rough and may partly explain the apparent concentration independence of the phase correlation lengths.

CONCLUSIONS

The phase behavior of PCBM in vinyl polymer matrices with different aromaticities have been investigated by means of DSC and SANS. The miscibility limit of PCBM in these polymers as defined by the loss of any crystallinity of the PCBM was found to increase non-linearly with

the number of aromatic moieties in the side chain with 16.5 wt.% in PS (1 aromatic ring), 57.0 wt.% in P2VN (2-fused aromatic rings) and 74.9 wt.% in P9VPh (3-fused aromatic rings). Below this miscibility limit a 'two-phase' morphology is seen in all three polymer-PCBM blends at all concentrations. However, the composition differences between these 'mixed' domains are very small and on average these mixed phases have comparatively small characteristic sizes.

Above the miscibility limit the phase domain sizes were found to be larger, but show weak dependence on the concentration and for each polymer were either approximately constant or increased slightly. The domains were found to have rough boundaries indicating either a large degree of randomness in size and shape, or diffuse interfaces between the phases. The scattering length density difference between the phases was however found to be dependent on the concentration for each polymer system. Even at the lowest concentration for each polymer distinct two-phase domain structures are observed although the difference in the concentration of the PCBM in either phase is small at the lowest concentration. As the overall PCBM content increases in the blend the concentration difference of the PCBM in each of the phases becomes more distinct. At a high concentration, DSC measurements indicate the presence of pure PCBM crystals in all the blends, with the remaining phase depleted of PCBM. The variation in miscibility of PCBM in the three polymers as determined by the DSC results is clearly reflected in the difference in the scattering length density values at the highest PCBM content samples measured. In this case PS demonstrates the greatest degree of partitioning of PCBM between the two phases so that when pure PCBM domains are present there is the least amount of PCBM remaining in the other phase. The opposite is true for the P9VPh system where, in comparison a large amount of PCBM is found in the remaining phase.

What is not immediately clear given our present results is the apparent origin of the 'two-phase' morphology in blends below the DSC derived miscibility limits. Whilst the very small scattering length density differences suggest density fluctuations, their origin is not known. It is entirely possible that the SANS is sensitive to very subtle phase behavior or composition fluctuations associated with the samples not being at true thermodynamic equilibrium. It is an important issue to understand and one that we are following up in future studies, especially since polymer-fullerene blends are widely used in organic electronics and the systems are never annealed to equilibrium.

REFERENCES AND NOTES

1. Sariciftci, N. S.; Braun, D.; Zhang, C.; Srdanov, V. I.; Heeger, A. J.; Stucky, G.; Wudl, F. *Applied Physics Letters* **1993**, *62*, 585.
2. Sariciftci, N. S.; Smilowitz, L.; Heeger, A. J.; Wudl, F. *Science* **1992**, *258*, 1474.
3. Yu, G.; Gao, J.; Hummelen, J. C.; Wudl, F.; Heeger, A. J. *Science* **1995**, *270*, 1789.
4. Troshin, P. A.; Hoppe, H.; Renz, J.; Egginger, M.; Mayorova, J. Y.; Goryochev, A. E.; Peregudov, A. S.; Lyubovskaya, R. N.; Gobsch,

G.; Sariciftci, N. S.; Razumov, V. F. *Advanced Functional Materials* **2009**, *19*, 779.

5. Lopez, A. M.; Mateo-Alonso, A.; Prato, M. *Journal of Materials Chemistry* **2011**, *21*, 1305.

6. Zhao, G.; He, Y.; Xu, Z.; Hou, J.; Zhang, M.; Min, J.; Chen, H.-Y.; Ye, M.; Hong, Z.; Yang, Y.; Li, Y. *Advanced Functional Materials* **2010**, *20*, 1480.

7. Matsumoto, F.; Moriwaki, K.; Takao, Y.; Ohno, T. *Synthetic Metals* **2010**, *160*, 961.

8. Mikroyannidis, J. A.; Kabanakis, A. N.; Sharma, S. S.; Sharma, G. D. *Advanced Functional Materials* **2011**, *21*, 746.

9. Treat, N. D.; Varotto, A.; Takacs, C. J.; Batara, N.; Al-Hashimi, M.; Heeney, M. J.; Heeger, A. J.; Wudl, F.; Hawker, C. J.; Chabinyc, M. L. *Journal of the American Chemical Society* **2012**, *134*, 15869.

10. Troshin, P. A.; Susarova, D. K.; Khakina, E. A.; Goryachev, A. A.; Borshchev, O. V.; Ponomarenko, S. A.; Razumov, V. F.; Sariciftci, N. S. *Journal of Materials Chemistry* **2012**, *22*, 18433.

11. Mueller, C.; Ferenczi, T. A. M.; Campoy-Quiles, M.; Frost, J. M.; Bradley, D. D. C.; Smith, P.; Stingelin-Stutzmann, N.; Nelson, J. *Advanced Materials* **2008**, *20*, 3510.

12. Kim, J. Y.; Frisbie, D. *Journal of Physical Chemistry C* **2008**, *112*, 17726.

13. Zhao, J.; Swinnen, A.; Van Assche, G.; Manca, J.; Vanderzande, D.; Van Mele, B. *Journal of Physical Chemistry B* **2009**, *113*, 1587.

14. Hopkinson, P. E.; Staniec, P. A.; Pearson, A. J.; Dunbar, A. D. F.; Wang, T.; Ryan, A. J.; Jones, R. A. L.; Lidzey, D. G.; Donald, A. M. *Macromolecules* **2011**, *44*, 2908.

15. Zhao, J.; Bertho, S.; Vandenbergh, J.; Van Assche, G.; Manca, J.; Vanderzande, D.; Yin, X.; Shi, J.; Cleij, T.; Lutsen, L.; Van Mele, B. *Physical Chemistry Chemical Physics* **2011**, *13*, 12285.

16. Ballantyne, A. M.; Ferenczi, T. A. M.; Campoy-Quiles, M.; Clarke, T. M.; Maurano, A.; Wong, K. H.; Zhang, W.; Stingelin-Stutzmann, N.; Kim, J.-S.; Bradley, D. D. C.;

Durrant, J. R.; McCulloch, I.; Heeney, M.; Nelson, J.; Tierney, S.; Duffy, W.; Mueller, C.; Smith, P. *Macromolecules* **2010**, *43*, 1169.

17. Bernardo, G.; Bucknall, D. G. *Recent Progress in the Understanding and Manipulation of Morphology in Polymer: Fullerene Photovoltaic Cells*, in *Optoelectronics - Advanced Materials and Devices* eds S.L. Pyshkin and J.M. Ballato, InTech**,** 2013.

18. Toropova, A. P.; Toropov, A. A.; Benfenati, E.; Gini, G.; Leszczynska, D.; Leszczynski, J. *Molecular Diversity* **2011**, *15*, 249.

19. Bucknall, D. G.; Bernardo, G.; Shofner, M. L.; Nabankur, D.; Raghavan, D.; Sumpter, B. G.; Sides, S.; Huq, A.; Karim, A. In *Polymer Composite Materials: From Macro, Micro to Nanoscale*; Boudenne, A., Ed.; Trans Tech Publications Ltd: Stafa-Zurich, 2012; Vol. 714, p 63.

20. Campbell, K.; Gurun, B.; Sumpter, B. G.; Thio, Y. S.; Bucknall, D. G. *Journal Of Physical Chemistry B* **2011**, *115*, 8989.

21. Sanz, A.; Wong, H. C.; Nedoma, A. J.; Douglas, J. F.; Cabral, J. T., *Polymer* **2015,** *68*, 47-56.

22. http://www.isis.stfc.ac.uk/

23. http://www.mantidproject.org/Main_Page

24. Wignall, G. D.; Bates, F. S. *Journal of Applied Crystallography* **1987**, *20*, 28.

25. http://www.sasview.org

26. Mens, R.; Chambon, S.; Bertho, S.; Reggers, G.; Ruttens, B.; D'Haen, J.; Manca, J.; Carleer, R.; Vanderzande, D.; Adriaensens, P. *Magnetic Resonance in Chemistry* **2011**, *49*, 242.

27. Pereira, P.; Gaspar, H.; Fernandes, L.; Bernardo, G., *Polymer Testing* **2015,** *47*, 130-136

28. Hammouda, B. *Polymer Reviews* **2010**, *50*, 14.

29. Debye, P.; Bueche, A. M. *Journal of Applied Physics* **1949**, *20*, 518.

30. Debye, P.; Anderson, H. R.; Brumberger, H. *Journal of Applied Physics* **1957**, *28*, 679.

31. Mildner, D. F. R.; Hall, P. L. *Journal of Physics D-Applied Physics* **1986**, *19*, 1535